Discrete Donor-Acceptor Pair Transitions in CH3NH3PbI3 Perovskite Single Crystals

Joanna M Urban, Trang Thi Huyen Nguyen, Gabriel Chehade, Aymeric Delteil, Gaëlle Trippé-Allard, Geraud Delport, Emmanuelle Deleporte, Jean-Pierre Hermier, Damien Garrot

Discrete Donor-Acceptor Pair Transitions in $CH_3NH_3PbI_3$ Perovskite Single Crystals

*Joanna M. Urban Trang Thi Huyen Nguyen Gabriel Chehade Aymeric Delteil Gaëlle Trippé-Allard Geraud Delport Emmanuelle Deleporte Jean-Pierre Hermier Damien Garrot**

Joanna M. Urban,[1] Gaëlle Allard-Trippé, Gabriel Chehade, Emmanuelle Deleporte
Université Paris-Saclay, ENS Paris-Saclay, CentraleSupélec, CNRS, LuMIn, F-91190 Gif-sur-Yvette, France
Géraud Delport
CNRS,UMR 9006,IPVF, Institut Photovoltaïque d'Ile-de-France 18 Boulevard Thomas Gobert, Palaiseau 91120, France
Trang Thi Huyen Nguyen, Aymeric Delteil, Jean-Pierre Hermier, Damien Garrot*
Université Paris-Saclay, UVSQ, CNRS, GEMaC, 78000, Versailles, France
Email Address: damien.garrot@uvsq.fr

Keywords: *halide perovskite, exciton, donor-acceptor pair, photoluminescence, defects*

Achieving a better understanding of the physics of defects in halide perovskites is a key challenge for improving the efficiency of the devices. Here, we present a comprehensive study of the defect emission of $CH_3NH_3PbI_3$ perovskite single crystals. The emission of the pristine surface of cleaved crystals is systematically investigated based on steady-state and time-resolved micro-photoluminescence spectroscopy. Donor-acceptor pair (DAP) recombination is observed due to the presence of native shallow defects. The DAP spectra present an important variability depending on the location on the surface of the crystals due to inhomogeneous defect distribution. A strong blue-shift of the emission is measured as a function of excitation power and is explained by fluctuating potential caused by compensated defects. With increasing photocarrier density, a transition from a structureless to a structured DAP emission with several longitudinal optical (LO) phonon replicas is observed. The DAP transition is characterized by the red-shift of the emission with time and a slow, non-exponential photoluminescence decay. Sharp discrete lines with sub-meV widths, the most recognizable spectral signature of DAP transition, are revealed. The results reconcile apparently contradictory previous observations on defect emission of $CH_3NH_3PbI_3$ and provide new insights into the properties of defects in halide perovskites.

1 Introduction

Halide perovskites (HPs) have demonstrated remarkable potential for photovoltaic and optoelectronic applications. The spectacular increase in the demonstrated power conversion

[1] Currently at Fritz Haber Institute of the Max Planck Society, 14195 Berlin, Germany

This article has been accepted for publication and undergone full peer review but has not been through the copyediting, typesetting, pagination and proofreading process, which may lead to differences between this version and the Version of Record. Please cite this article as doi: 10.1002/pssr.202300005.

efficiency, which has recently exceeded 25%, [1] makes 3D HPs very attractive as light-harvesting materials in solar cells. Their excellent light emission properties are highly interesting for applications in light emitting diodes,[2, 3] lasers,[4, 5, 6] photodetectors and other devices.[7]

However, the understanding of some of the fundamental processes governing the photophysical properties of HPs is still incomplete. In particular, many open questions remain regarding the influence of defects in these materials on the electronic structure and carrier dynamics. Solution-based synthesis, which makes perovskites so promising from the perspective of low-cost photovoltaics, typically leads to a high concentration of defects in the crystal lattice.[8]

In stark contrast to classical semiconductor materials, the presence of such a significant number of lattice imperfections does not strongly impact the perovskite material performance.[9, 10, 11] HPs show surprising defect tolerance and are characterized by high power conversion efficiency, long carrier lifetimes and long carrier diffusion lengths.[9, 12] The apparent defect tolerance of HPs is assumed to be due to the fact that the native defects with lowest formation energies would induce shallow levels, as predicted by Density Functional Theory (DFT) calculations.[13, 14, 15] Nonetheless, for HPs to reach their full potential, it is crucial to fully understand and reduce any detrimental influence of defects. Avoidable nonradiative recombination losses are the main obstacle to be eliminated on the path to approaching the theoretical Shockley–Queisser limit for solar-cell efficiencies.[16] Additionally, intrinsic defects can be used to achieve controllable electrical doping in HPs.[17, 18, 19] A better understanding and control of the defect and impurity states are crucial to the development of electronic devices based on HPs.[20, 21, 22]

Low temperature photoluminescence (PL) spectroscopy is a powerful technique to study the defects and impurities in semiconductors. However, concerning halide perovskites, despite numerous studies, there is no consensus on the origin of the low temperature defect emission. The Free Excitonic (FE) emission has been identified by some of us in the PL spectra of $CH_3NH_3PbI_3$ single crystals,[23] and in a few other studies.[24, 25, 26] However, in many cases, the low temperature optical spectra of 3D HPs are characterized by the presence of several overlapping broad and featureless bands at energies below the FE emission. The low-energetic emission features have been assigned to various phenomena: bound excitons,[27] tetragonal phase inclusions,[28, 29, 30] Donor-acceptor pair recombination,[31] molecularly disordered orthorhombic domains,[32] or band tail emission.[33] More structured spectra have been recently reported, in particular showing narrow peaks with meV width assigned to excitons bound to shallow defects.[25]

One of the main difficulties in understanding the low temperature emission of hybrid perovskites is related to the solution processing. Optoelectronic properties depend on the synthesis method and its impact on the microstructure.[34] Inside the material, large local fluctuations of the defect density at different length scales are observed.[35] Polycrystalline thin films present an average trap density of 10^{16}-10^{17} cm^{-3}. In comparison, single crystals present a defect density four orders of magnitude lower, of the orders of 10^{11} cm^{-3} and are considered to be the best platform to study the fundamental properties of hybrid perovskites. [36, 37] However, even single crystals are not exempt from disorder and heterogeneity.[38] Ni *et al.* show in particular that the concentration of defect-induced trap states varies by five orders of magnitude between the surface and bulk of crystals.[39] The heterogeneity of the material is reflected in the low temperature emission of $CH_3NH_3PbI_3$. PL spectroscopy of single crystals leads to apparently contradictory results with reports of only featureless broadband emission on the one hand and of sharp excitonic emission on the other hand.[27, 23, 25, 40]

Here, to better understand the defect emission in $CH_3NH_3PbI_3$, we have systematically

investigated the PL of multiple $CH_3NH_3PbI_3$ crystals at low temperature, at the microscale, based on power dependence and time-resolved micro-photoluminescence. Below the energy of the free exciton, both structureless and well-structured emission features are observed depending on the surface quality and excitation power. The spatial inhomogeneity of the emission is assigned to the local variation of the defect density. The compensation effect of native charged defects induces potential fluctuations. The latter are responsible for the observation of a large blue-shift of the defect emission with increasing excitation power. In lower defect density regions and/or at higher excitation power, a structured DAP emission with well-defined LO-phonon replicas is evidenced. We have analyzed the time-resolved spectra of the DAP emission, characterized by a large redshift. The time-resolved PL dynamics shows non-exponential decays, which can be approximated by a power law. Finally, we highlight the fine structure of DAP emission, observed on cleaved crystal surfaces. The high energy side of the DAP emission presents a characteristic series of narrow lines with sub-meV widths. We observe the thermal quenching of these features due to ionization of the donor/acceptor shallow states with low energy of approximately 4 meV.

2 Results and discussion

2.1 Excitation power dependence of the PL spectra

We measured the low-temperature photoluminescence spectra of single crystals of $CH_3NH_3PbI_3$, the archetypal 3D HPs (**Figure 1a**). We prepare pristine surfaces by cleaving the crystals.[41, 42] Applying pressure with a tweezer, we break the crystals into fragments. In comparison with the surface of as-grown crystals, which can be rough and inhomogeneous, cleaved fragments present smooth, mirror-like surfaces (**Figure S1**). Below 160 K, the crystal structure of $CH_3NH_3PbI_3$ is orthorhombic with Pnma space group.[43, 44] **Figure 1b** shows the reflectivity and photoluminescence spectra measured at 5 K. The free excitonic emission (FE) has a maximum at 1.637 eV and presents a shape very close to a Lorentzian with a full width at half maximum (FWHM) of only 3 meV. The emission presents a very good correspondence with the excitonic transition measured in reflectivity. The narrow linewidth of the FE indicates the good crystalline quality of the material.[45] The reflectivity spectrum presents an inflection point at 1.637eV approximately in good agreement with previous reports.[46, 26]

It is now well-established that excitons in $CH_3NH_3PbI_3$ have a low binding energy, estimated as approximately 15 meV in the low temperature orthorhombic phase, and a few meV in the room temperature tetragonal phase.[47, 48] While free carriers are predominantly generated upon photoexcitation at room temperature, we can expect excitons to be stable in the low temperature phase.[49]

To the best of our knowledge, a narrow free excitonic emission has never been observed in polycrystalline thin films, and it is not always visible even in studies performed on single crystals.[27, 40] Broadband emissions, with FWHM of several hundred of meV, are generally reported.[28] Here, as shown in **Figure 1b**, the free excitonic emission can be observed with almost no contribution at low energy.

However, we observe strong spatial variations of the micro-PL for different positions on the same crystal. PL Map and additional spectra are presented on **Figure S2**. Depending on the local position on the crystal, a broadband emission and several sharp peaks, below the FE energy, can be observed. The FE emission can be completely quenched in the presence of a strong defect emission.

Next, we have investigated the excitation power dependence of the emission. The low energy band depends strongly on the excitation power. **Figure 2a** shows a series of normalized micro-PL spectra for different excitation powers at 5K. Additional spectra are shown in **Figure S5**. In addition

to the FE emission, different features are observed at low energy. A series of sharp peaks is visible, at 1.633 eV and 1.618 eV. These structures are assigned to Free-to-Bound (FB) transitions and Bound Excitons (BE) respectively, as explained below. The BE band presents a substructure with three peaks, mainly visible at low excitation power (**Figure S3**). The width of these emission lines is approximately 2 meV. They broaden and begin to overlap with increasing excitation power. At an excitation power of 0.022 µW, the broad band is visible between approximately 1.54 and 1.61 eV, with a FWHM of approximately 55 meV. We assign this band to DAP recombination for the reasons detailed below.

The positions of the BE peaks remain unchanged with increasing excitation power. The energy of the FB peak presents a slight blue shift of a few meV at very low excitation power (**Figure S4)** and is stable at higher excitation power. In contrast, we can observe a large blueshift of the broad lower-energetic band. As the excitation power increases the broad band shifts to higher energy and overlaps with the BE peaks. The energy of the broadband emission maximum is approximately 1.594 eV at 0.022 µW and reaches 1.630 eV for the highest excitation powers (29.9 µW). It presents also a strong saturation in intensity with increasing excitation power. The evolution as a function of excitation power of the PL intensity at different energies, characteristic of the different spectral features is displayed in **Figure 2b**. For the DAP band, the PL Intensity has been measured at 1.600 eV. The evolution of the FE and BE intensity can be described with a power law $I \propto P^{\lambda}$ with $\lambda > 1$ as expected for excitonic transitions.[50] Value of λ close to or inferior to one are characteristic of FB and DAP recombination. The broadband emission intensity could not be described with a single power law as it shifts and saturates at high power.

Different mechanisms can induce a blue-shift of the PL with increasing excitation power. The power-dependent blue-shift of the low energy broadband emission of $CH_3NH_3PbI_3$ has been assigned to band filling effect[32], redistribution of carriers from trap states to excitonic emission[27], saturation of tetragonal phase inclusions[28] or DAP recombination.[51, 31]

Depending on their electronic properties, point defects and impurities can be donors or acceptors. Donor-acceptor pair transitions refer to a radiative recombination process between an electron on a donor and a hole on an acceptor, leading to the formation of ionized species D^+ and A^- (**Figure 2d**).[52] The ionized donors (D^+) and acceptors(A^-) return to the neutral state (D^o, A^o) by capturing photocarriers .

$$D^0 + A^0 \rightarrow D^+ + A^- + photon \quad (1)$$

The energy of the emitted photons is given by :

$$h\nu_{(D^0-A^0)} = E_g - (E_D + E_A) + \frac{e^2}{4\pi\epsilon\epsilon_0 R} - m\hbar\omega_{LO} \quad (2)$$

where E_g is the bandgap energy of the semiconductor, E_D and E_A are the binding energies, $\frac{e^2}{4\pi\epsilon\epsilon_0 R}$ is the mutual electrostatic attraction between the charged pair, with ϵ_0 the vacuum permittivity and ϵ the low frequency relative dielectric constant of the semiconductor. R in the Coulombic interaction term is the distance between donor and acceptor, determined by the crystal structure and lattice constant. Consequently, close DA pairs will emit at higher energy than distant pairs. The last term accounts for LO phonon replicas.

As the excitation power increases, acceptors and donors are saturated and the probability of observing a radiative recombination from a close pair increases. The emission shifts toward higher

energy. However, DAP recombination generally induces blue-shift of the order of a few meV per decade of excitation power.[53] The blueshift observed in the dataset shown in **Figure 2c** is significantly larger. The band maximum shifts from 1.594 eV to 1.630 eV within the investigated excitation power range, yielding a blueshift around 20 meV per decade (**Figure 2c** and **Figure S5**).

An analytical expression has been derived for the shift of the DAP emission as a function of excitation power (P_{exc}) for the case of a transition between a shallow impurity and a deeper one.[53]

$$P_{exc} \propto \frac{(E-E_{\infty})^3}{E_B+2E_{\infty}-2E}\exp(-\frac{2E_B}{E-E_{\infty}}) \quad (3)$$

where $E_{\infty} = E_g - E_A - E_D$ is the limiting photon energy of for an infinitely distant pair, $E_B = e^2 / 4\pi\epsilon\epsilon_0 R_B$ with R_B the Bohr radius of the shallow defect. E can vary between E_{∞} and $\frac{1}{2}(E_B + 2E_{\infty})$.

A fit of the data is shown in **Figure 2c**. The model can only fit correctly the high energy part of the data. A limiting value at high excitation power is clearly seen. The extracted value of $E_A + E_D \approx 90\,\text{meV}$ is in good agreement with the presence of shallow defects.[15, 54]

To explain the observation of a large blue-shift, we have to consider potential fluctuations. The latter appear in strongly compensated semiconductors.[55] In a compensated semiconductor, most of the donors and acceptors are charged at low excitation power and, in consequence, they induce Coulomb-potential fluctuations, creating local minima/maxima in the valence and conduction band. Both interband transitions and DAP transitions are red-shifted in comparison to the flatband situation proportionally to the potential depth (**Figure 2e**). With increasing excitation power, the potential fluctuations are progressively screened by the photogenerated carriers and a strong blue-shift is observed, of the order of the potential depth.

The influence of potential fluctuations on the PL has been studied in different inorganic semiconductors.[56, 57] The potential fluctuation depth is dependent on the density of donor/acceptor and level of compensation.[58] The observation of potential fluctuations at low temperature is consistent with the importance of Schottky disorder in hybrid perovskites.[59, 60] This type of defect will lead to the creation of a stoichiometric quantity of anion and cation vacancies, randomly distributed in the crystal, leading to compensated donors and acceptors.

An energy-shift constant β has been defined to describe the blue-shift of DAP band in strongly compensated semiconductors such that:[61]

$$P_{exc} = P_0 \exp(E/\beta) \quad (4)$$

where P_0 is a fitting parameter. From the fit of the low excitation power data (**Figure 2c**), we have extracted a value of $\beta \approx 12\,\text{meV}$. Comparable values have been reported for Cu_2ZnSnS_4 (CZTS) and $Cu(In,Ga)Se_2$ (CIGS).[62, 63]

Potential fluctuations may also explain the blue-shift of the FB peak observed at low excitation power. The emission of FB transition is otherwise expected to be stable in energy and is blue-shifted in comparison to DAP emission (**Figure 2d**).

$$h\nu_{FB} = E_g - E_{D/A} \quad (5)$$

The spectra of the two recombination mechanisms often overlap.[64] The tentative assignment of the peak at 1.633 eV to FB transition leads to an estimated $E_{D/A} = 19\ \text{meV}$ which is consistent with our estimated value of $E_A + E_D \approx 90\ \text{meV}$.

With increasing photocarrier density and screening of the potential fluctuations, we may expect a transition from featureless DAP emission, red-shifted due to band bending, to the characteristic features of DAP recombination in a weakly compensated semiconductor. Indeed, as the excitation power increases, we observe the crossover from a structureless broad band to a well-structured emission presenting phonon replicas. The spectrum measured at a power of 0.24 μW is reproduced on **Figure 3a**. It presents the DAP band on top of which several evenly spaced peaks appear.

We assigned this structure to the LO-phonon replicas of the DAP transition. The spacing of approximately 4.3 meV is in excellent agreement with the optical phonon energy extracted from the temperature dependent PL lineshape broadening measurements on $CH_3NH_3PbI_3$ single crystals by some of us and other authors.[23, 25, 40]

In 3D HPs, electron-phonon coupling is expected to be dominated by interaction with LO-phonons via the Fröhlich mechanism. A 4 meV LO-phonon energy has been measured at 5 K with inelastic neutron scattering and Raman scattering.[65] This low energy phonon mode is associated to the inorganic sublattice and would correspond to the bending of the PbX_3 network.[66] Interestingly, strong coupling of the optical band gap to a mode at this frequency has also been reported.[67] The phonon replicas are less apparent at higher power as the DAP band overlaps with the BE emission.

The presence of LO-phonon replicas of the DAP band is even more apparent on the spectrum in **Figure 3b** recorded in another region of the sample, presenting a stronger DAP emission where a modulation of broad band emission with a spacing of 4.3 meV is well resolved. A strong coupling with LO-phonons is a characteristic of DAP emission in many semiconductors.[68, 69, 56] The transition with increasing excitation power or doping from redshifted structureless DAP emission to a well defined DAP emission accompanied by LO-phonon replicas was observed in different materials.[56]

We note that the intensity of the LO-phonon replicas, characterized by the Huang-Rhys factor, is dependent of the distance between donors and acceptors, and is predicted to decrease with the pair separation.[70, 71] The average distance between localized carriers and in consequence the intensity of the replicas change with the excitation power. The decrease of the Huang-Rhys factor with increasing excitation power may also explain why the phonon replicas are less visible in the high excitation regime.

2.2 Time-resolved spectroscopy

To further elucidate the origin of the defect emission, we study the time evolution of the emission. First, we compare the lifetime of the FE and the broad band. The FE decays with an initial lifetime of approximately 330 ps which can be assigned to the exciton lifetime (**Figure 4a**).[72] This fast initial decay is followed by a longer component spanning over several hundreds of nanoseconds. The long component can be described by a power law decay: $PL(t) \propto t^{-\beta}$ with $\beta = 1$. Previously, a long microsecond lifetime observed in single crystals of $CH_3NH_3PbI_3$ has been assigned to bound triplet excitons.[27] However, the long lifetime can alternatively be explained by the presence of shallow defects, responsible for both carrier trapping/detrapping and donor-acceptor pair recombination.[73, 74, 51]

When the temperature is raised, the intensity of the delayed luminescence decreases due to detrapping from donor and acceptor levels (**Figure S6**). Tilchin *et al.* have reported a delayed luminescence of the free excitonic emission in single crystals of $CH_3NH_3PbBr_3$. The power law decay, with a β coefficient below 1, has been assigned to detrapping from shallow states or/and free electron-hole annihilation.[51] We observe that the broad DAP emission (measured here at 1.590 eV and 1.570 eV) also presents a power law decay: $PL(t) \propto t^{-\beta}$ with $\beta < 1$ (**Figure 4b**). The recombination rate decreases with the emission energy as expected for DAP recombination. The time dependence of the broad band emission is consistent with the hypothesis of the presence of shallow donor/acceptor inducing trapping/detrapping and DAP recombination. Non-exponential decays are characteristic of DAP emission.[68] They have been described by power laws, with β coefficient ranging between 0.7 to 2 in different inorganic semiconductors.[73, 75, 76, 77]

We now turn to the time-resolved spectra. **Figure 4c** and **4d** show an energy versus time map of the PL emission and **Figure 4e** displays spectra at different delays after the excitation pulse. Note that the spectral resolution for this measurement is approximately 1 nm (see supporting information). Nonetheless, we can identify the different structures previously reported in **Figure 2a**. We observe that the emission is initially dominated by the FE peak whose energy remains stable in time. We note that the spectra on **Figure 4e** are normalized: the fact that we still observe the FE peak spectra at several hundred of nanoseconds after pulsed excitation is due to delayed luminescence.

Simultaneously, we observe the emission of the BE peaks. The emission at approximately 1.63 eV, that we have assigned to Free-to-bound transition, builds up at longer times which indicates a slow capture probability. The emission of excitons bound to ionized defects has also been reported in a previous study in the same energy range.[25] The emission observed here presents a very slow dynamics which seems incompatible with the assignment to bound excitons, characterized by fast recombination rates.

The DAP band appears initially at 1.627 eV and strongly red-shifts with time. The band briefly overlaps with the BE emission and forms a broad emission at low energy on longer time-scale. Red-shift of emission energy as a function of time is another characteristic feature of DAP recombination. The radiative recombination probability of the electron of the donor and hole of the acceptor depends exponentially on their separation R as $\exp\left[-2\ R/a_{D,A}\ \right]$, where $a_{D,A}$ is the Bohr radius of the donor/acceptor. Closer DA pair will recombine faster and produce an emission at higher energy. With time, pairs at larger distance will recombine and the spectrum shift toward lower energy.[68] The energy span observed here in time-resolved emission between close and distant pairs is in very good agreement with the variation recorded as a function of excitation power.

2.3 Discrete donor-acceptor pairs emission and temperature dependence

We have previously highlighted several characteristic features of DAP recombination. However, the hallmark of DAP emission is the presence of numerous sharp lines induced by the Coulombic interaction between close distance pairs.

The spectrum in **Figure 5a** (see also **Figure S7**) presents the broad contribution previously described but with a series of sharp lines with sub-meV FWMH on the high energy side of the emission. The discrete lines emerge from the broad pair recombination background. **Figure 5b** presents a fit of one of the lines with a Lorentzian function with a 260 µeV FWHM. These sharp lines are found on the high energy side of the broad band contribution caused by distant pairs. Several hundreds of sharp lines have been observed in GaP.[68] Here, the low defect density of the cleaved crystals allows us to resolve the discrete pair transitions, whereas as-grown crystal surfaces present only overlapping pair emission. Multiple bound exciton complexes (MBEC) can be excluded as a possible mechanism for the emission: the main feature of MBEC is the apparition of several weaker satellites at lower energy of an intense emission.[78] Additional spectra, displaying similar sharp

structures are presented in **Figure S8**.

The temperature dependence of the emission is displayed on **Figure 5c**. As the temperature is raised, the sharp lines present a blue-shift. A blue shift with increasing temperature is characteristic of DAP emission.[25] However, as the band gap of $CH_3NH_3PbI_3$ increases with temperature,[23] we are not able here to distinguish the two phenomena. The intensity of the discrete lines decreases quickly, leaving only the broad band contribution visible at 20 K. We have plotted the intensity as function of temperature for the peak at 1.6154 eV in **Figure 5d**. The thermal behavior can be fitted with the formula:

$$I\ T\ = \frac{I_0}{1+Cexp(-E/k_BT)} \qquad (6)$$

The fit yields a value of the thermal activation energy $E = 4.2 \pm 0.5\,meV$. The value is close to the energy of the LO-Phonon mode previously found. The observation suggests a phonon assisted detrapping of charge carriers.

The assignment of the DAP emission to specific native point defects can be discussed based on the results of theoretical predictions. The formation energy and energy levels of native defects in $CH_3NH_3PbI_3$ have been calculated based on DFT calculations, in different studies.[15, 54, 8] The results suggest that defects with low formation energies create only shallow levels, rather than deep defects. Shallow defects which are expected to be most prevalent due to low formation energy are related to Vacancies (V) and Interstitials (i) point defects: V_{Pb}, V_{MA} for acceptor defects and V_I, MA_i, Pb_i for donor defects. Schottky defects, which create an equal number of positive and negative vacancies, such as PbI_2 and MAI vacancy have also been considered. Kim et al. have estimated that the formation energies of PbI_2 vacancies are substantially lower than those of MAI vacancies and suggested that they are likely abundant in HPs.[14] Despite the progress in the theoretical description of defects in HPs, there are still discrepancies in the reported nature, shallow or deep level, of some defects in $CH_3NH_3PbI_3$.[79] The observation of the spectral signature of discrete DAPs is an important step in the characterization of defects in HPs.

Additionally, single photon emission has been recently reported from localized states in $CH_3NH_3PbI_3$ nanocrystals and $CsPbBr_3$ microcrystals, but the physical origin of emitters is still unclear.[80, 81] DAP transitions have been suggested as the main origin of single-photon emitters in hBN in a recent study [82] and could be the possible mechanism for the previously reported quantum emitters in HPs. Interestingly, understanding the nature of defect-related states is also relevant to application in lasing since these states are implied in the mechanism of lasing in halide perovskites.[83]

2.4 Conclusion

To summarize, we have shown that the low temperature defect emission of $CH_3NH_3PbI_3$ presents important variations which can be understood in the context of DAP recombination. Both structureless and well-structured emission bands can be observed. We assign the observed variations in the emission of single crystals to a significant inhomogeneity in the defect density. Potential fluctuations due to compensated native defects cause the broadening of the emission into a large structure-less band characterized by a strong power dependent redshift in regions with high defect density, while structured DAP emission with LO-phonon replica can be recorded in lower defect density regions or at higher excitation power. The presence of shallow donor/acceptor defects lies at the origin of the long lived low-energy luminescence following a power law decay. The characteristic fine structure of discrete donor-acceptor pair emission, with sub-meV linewidth, is highlighted. Our

results shed a new light on the contrasting observations reported in the literature and the difficulty in reaching a consensus regarding the defect emission. We highlight the importance of a systematic study at the microscale of the emission of crystal due to the inhomogeneous nature of the material. In addition to the excitation power dependence and time-resolved dynamics, the observation of discrete lines at high energy is the fingerprint of DAP recombination. Altogether our comprehensive study of the emission of $CH_3NH_3PbI_3$ explains the seemingly contradictory previous observations and provides strong evidence that DAP recombination is at the origin of the broad low energy emission band in $CH_3NH_3PbI_3$. The results pave the way for a deeper experimental characterization of native defects in HPs which is crucial for the further development of optoelectronics devices.

3 Methods

Crystal growth and sample preparation:

We performed the measurements on high quality $CH_3NH_3PbI_3$ single crystals grown using a solution-based method. Methylammonium iodide (0.78 g, 5 mmol) and lead iodide (2.30 g, 5 mmol) were dissolved in GBL (5 mL) at 60°C. 2 mL of the yellow solution was placed into a vial and heated at 120°C during one to four hours depending on the crystals size expected. The solution could be heated in a hot plate as well as an oil bath. The crystals were mechanically cleaved directly before mounting in the cryostat for optical measurements to expose a clean fresh surface unaltered by degradation in ambient conditions.

Optical characterization:

The samples were placed in the confocal microscope insert of a top-loading closed-cycle cryostat (AttoDRY 1100). The measurements were performed in exchange gas atmosphere and the excitation was provided either by a 485 nm or 520 nm picosecond laser diode (PDL 800-D PicoQuant). The collected signal was dispersed using an ACTON SpectraPro 2750 spectrometer and recorded on a CCD camera (Pixis100, Princeton Instruments).

For time-resolved measurements, the signal was recorded using an avalanche photodiode (PicoQuant PDM series) and the PicoHarp 300 Time-Correlated Single Photon Counting system. For spectrally resolved measurements of the PL lifetime, the signal passed through a Fourier-transform interferometer (NIREOS GEMINI) before being recorded by the photodiode.

Acknowledgements

This work was financially supported by the French National Research Agency (ANR EMIPERO, ANR-18-CE24-0016, ANR HYPERSOL ANR-18-CE05-0021 and ANR MARS, ANR-20-CE92-0041-03).

References

[1] J. Y. Kim, J.-W. Lee, H. S. Jung, H. Shin, N.-G. Park, *Chemical Reviews* **2020**, *120*, 15 7867.

[2] C. Ge, Q. Fang, H. Lin, H. Hu, *Frontiers in Materials* **2021**, *8* 635025.

[3] L. Zhang, C. Sun, T. He, Y. Jiang, J. Wei, Y. Huang, M. Yuan, *Light: Science & Applications* **2021**, *10*, 1 61.

[4] G. Xing, N. Mathews, S. S. Lim, N. Yantara, X. Liu, D. Sabba, M. Gratzel, S. Mhaisalkar,

T. C. Sum, *Nature Materials* **2014**, *13*, 5 476.

[5] P. Bouteyre, H. S. Nguyen, J.-S. Lauret, G. Trippé-Allard, G. Delport, F. Lédée, H. Diab, A. Belarouci, C. Seassal, D. Garrot, F. Bretenaker, E. Deleporte, *Optics Express* **2020**, *28*, 26 39739.

[6] L. Lei, Q. Dong, K. Gundogdu, F. So, *Advanced Functional Materials* **2021**, *31*, 16 2010144.

[7] C. Xie, C.-K. Liu, H.-L. Loi, F. Yan, *Advanced Functional Materials* **2019**, *30*, 20 1903907.

[8] J. M. Ball, A. Petrozza, *Nature Energy* **2016**, *1*, 11 16149.

[9] Y. Guan, X. Zhang, G. Nan, *Physical Chemistry Chemical Physics* **2021**, *23*, 11 6583.

[10] P. Nandi, C. Giri, D. Topwal, *Journal of Materials Chemistry C* **2021**, *9*, 8 2793.

[11] W. Chu, Q. Zheng, O. V. Prezhdo, J. Zhao, W. A. Saidi, *Science Advances* **2020**, *6*, 7 eaaw7453.

[12] A. Forde, D. Kilin, *Journal of Chemical Theory and Computation* **2021**, *17*, 11 7224.

[13] N. Liu, C. Yam, *Physical Chemistry Chemical Physics* **2018**, *20*, 10 6800.

[14] J. Kim, S.-H. Lee, J. H. Lee, K.-H. Hong, *The Journal of Physical Chemistry Letters* **2014**, *5*, 8 1312.

[15] W.-J. Yin, T. Shi, Y. Yan, *Applied Physics Letters* **2014**, *104*, 6.

[16] D. Luo, R. Su, W. Zhang, Q. Gong, R. Zhu, *Nature Reviews Materials* **2019**, *5*, 1 44.

[17] Q. Wang, Y. Shao, H. Xie, L. Lyu, X. Liu, Y. Gao, J. Huang, *Applied Physics Letters* **2014**, *105*, 16 163508.

[18] J. Euvrard, Y. Yan, D. B. Mitzi, *Nature Reviews Materials* **2021**, *6*, 6 531.

[19] P. Cui, D. Wei, J. Ji, H. Huang, E. Jia, S. Dou, T. Wang, W. Wang, M. Li, *Nature Energy* **2019**, *4*, 2 150.

[20] O. F. Ngome Okello, D.-H. Yang, Y.-S. Chu, S. Yang, S.-Y. Choi, *APL Materials* **2021**, *9*, 10 100902.

[21] C. Chakraborty, L. Kinnischtzke, K. M. Goodfellow, R. Beams, A. N. Vamivakas, *Nature Nanotechnology* **2015**, *10*, 6 507.

[22] Rosa Brakkee, Rene M Williams, *Applied Sciences* **2020**, *10*, 9 3061.

[23] H. Diab, G. Trippé-Allard, F. Lédée, K. Jemli, C. Vilar, G. Bouchez, V. L. Jacques, A. Tejeda, J. Even, J.-S. Lauret, E. Deleporte, D. Garrot, *The Journal of Physical Chemistry Letters* **2016**, *7*, 24 5093.

[24] L. Q. Phuong, Y. Nakaike, A. Wakamiya, Y. Kanemitsu, *The Journal of Physical*

Chemistry Letters **2016**, 4905–4910.

[25] A. Francisco-López, B. Charles, M. I. Alonso, M. Garriga, M. T. Weller, A. R. Goñi, *Advanced Optical Materials* **2021**, *9*, 18 2001969.

[26] R. S. Nazarov, I. A. Solovev, A. O. Murzin, N. I. Selivanov, J. Even, A. V. Emeline, Y. V. Kapitonov, *Physical Review B* **2022**, *105*, 24 245202.

[27] H.-H. Fang, R. Raissa, M. Abdu-Aguye, S. Adjokatse, G. R. Blake, J. Even, M. A. Loi, *Advanced Functional Materials* **2015**, *25*, 16 2378.

[28] C. Wehrenfennig, M. Liu, H. J. Snaith, M. B. Johnston, L. M. Herz, *APL Materials* **2014**, *2*, 8 081513.

[29] F. Panzer, S. Baderschneider, T. P. Gujar, T. Unger, S. Bagnich, M. Jakoby, H. Bässler, S. Hüttner, J. Köhler, R. Moos, M. Thelakkat, R. Hildner, A. Köhler, *Advanced Optical Materials* **2016**, *4*, 6 917.

[30] K. Galkowski, A. A. Mitioglu, A. Surrente, Z. Yang, D. K. Maude, P. Kossacki, G. E. Eperon, J. T.-W. Wang, H. J. Snaith, P. Plochocka, R. J. Nicholas, *Nanoscale* **2017**, *9*, 9 3222.

[31] W. Kong, Z. Ye, Z. Qi, B. Zhang, M. Wang, A. Rahimi-Iman, H. Wu, *Phys. Chem. Chem. Phys.* **2015**, *17*, 25 16405.

[32] M. I. Dar, G. Jacopin, S. Meloni, A. Mattoni, N. Arora, A. Boziki, S. M. Zakeeruddin, U. Rothlisberger, M. Grätzel, *Science Advances* **2016**, *2*, 10 e1601156.

[33] N. Shrestha, Z. Song, C. Chen, E. Bastola, X. Wang, Y. Yan, R. J. Ellingson, *The Journal of Physical Chemistry Letters* **2019**, *11*, 1 121.

[34] A. R. Srimath Kandada, A. Petrozza, *Accounts of chemical research* **2016**, *49*, 3 536.

[35] E. M. Tennyson, T. A. S. Doherty, S. D. Stranks, *Nature Reviews Materials* **2019**, *4*, 9 573.

[36] V. Adinolfi, M. Yuan, R. Comin, E. S. Thibau, D. Shi, M. I. Saidaminov, P. Kanjanaboos, D. Kopilovic, S. Hoogland, Z.-H. Lu, O. M. Bakr, E. H. Sargent, *Advanced Materials* **2016**, *28*, 17 3406.

[37] Y. Chen, H. T. Yi, X. Wu, R. Haroldson, Y. N. Gartstein, Y. I. Rodionov, K. S. Tikhonov, A. Zakhidov, X. Y. Zhu, Podzorov., *Nature Communications* **2016**, *7* 12253.

[38] M. Gerhard, B. Louis, P. A. Frantsuzov, J. Li, A. Kiligaridis, J. Hofkens, I. G. Scheblykin, *Advanced Optical Materials* **2021**, 2001380.

[39] Z. Ni, C. Bao, Y. Liu, Q. Jiang, W.-Q. Wu, S. Chen, X. Dai, B. Chen, B. Hartweg, Z. Yu, Z. Holman, J. Huang, *Science* **2020**, *367*, 6484 1352.

[40] I. V. Zhevstovskikh, N. S. Averkiev, M. N. Sarychev, O. I. Semenova, O. E. Tereshchenko, *Journal of Physics D: Applied Physics* **2021**, *55*, 9 095105.

[41] H. Ryu, J. Park, S. H. Nam, J. W. Park, K. Kim, Y. Yi, J. I. Jang, *Advanced Materials*

2022, 2107882.

[42] M. Kollár, L. Ćirić, J. H. Dil, A. Weber, S. Muff, H. M. Ronnow, B. Náfrádi, B. P. Monnier, J. S. Luterbacher, L. Forró, E. Horváth, *Scientific Reports* **2017**, *7*, 1 695.

[43] T. Baikie, Y. Fang, J. M. Kadro, M. Schreyer, F. Wei, S. G. Mhaisalkar, M. Graetzel, T. J. White, *Journal Of Materials Chemistry A* **2013**, *1*, 18 5628.

[44] M. T. Weller, O. J. Weber, P. F. Henry, A. M. Di Pumpo, T. C. Hansen, *Chem. Commun.* **2015**, Advance.

[45] N. I. Selivanov, A. O. Murzin, V. I. Yudin, Y. V. Kapitonov, A. V. Emeline, *CrystEngComm* **2021**, *24*, 16 2976.

[46] Y. Yamada, H. Mino, T. Kawahara, K. Oto, H. Suzuura, Y. Kanemitsu, *Physical Review Letters* **2021**, *126*, 23 237401.

[47] A. Miyata, A. Mitioglu, P. Plochocka, O. Portugall, J. T.-W. Wang, S. D. Stranks, H. J. Snaith, R. J. Nicholas, *Nature Physics* **2015**, *11*, 7 582.

[48] Q. Lin, A. Armin, R. C. R. Nagiri, P. L. Burn, P. Meredith, *Nature Photonics* **2015**, *9* 106.

[49] M. Saba, F. Quochi, A. Mura, G. Bongiovanni, *Accounts of Chemical Research* **2015**, acs.accounts.5b00445.

[50] T. Schmidt, K. Lischka, W. Zulehner, *Physical Review B* **1992**, *45*, 16 8989.

[51] J. Tilchin, D. N. Dirin, G. I. Maikov, A. Sashchiuk, M. V. Kovalenko, E. Lifshitz, *ACS Nano* **2016**, *10*, 6 6363.

[52] P. Y. Yu, M. Cardona, *Fundamentals of Semiconductors*, Graduate Texts in Physics. Springer Berlin Heidelberg, **2010**.

[53] E. Zacks, A. Halperin, *Physical Review B* **1972**, *6*, 8 3072.

[54] D. Meggiolaro, S. G. Motti, E. Mosconi, A. J. Barker, J. Ball, C. Andrea Riccardo Perini, F. Deschler, A. Petrozza, F. De Angelis, *Energy & Environmental Science* **2018**, *11*, 3 702.

[55] B. I. Shklovskii, A. L. Efros, *Electronic Properties of Doped Semiconductors*, Springer Berlin Heidelberg, **1984**.

[56] P. Bäume, J. Gutowski, D. Wiesmann, R. Heitz, A. Hoffmann, E. Kurtz, D. Hommel, G. Landwehr, *Applied Physics Letters* **1995**, *67*, 13 1914.

[57] M. Reshchikov, H. Morkoc, *Journal Of Applied Physics* **2005**, *97*, 6.

[58] M. Behringer, P. Bäume, J. Gutowski, D. Hommel, *Physical Review B* **1998**, *57*, 20 12869.

[59] A. Walsh, D. O. Scanlon, S. Chen, X. G. Gong, S.-H. Wei, *Angewandte Chemie International Edition* **2015**, *54*, 6 1791.

[60] C. C. Stoumpos, C. D. Malliakas, M. G. Kanatzidis, *Inorganic Chemistry* **2013**, *52*, 15 9019.

[61] P. W. Yu, Y. S. Park, *Journal of Applied Physics* **1977**, *48*, 6 2434.

[62] J. P. Teixeira, R. A. Sousa, M. G. Sousa, A. F. da Cunha, P. A. Fernandes, P. M. P. Salomé, J. C. González, J. P. Leitão, *Applied Physics Letters* **2014**, *105*, 16 163901.

[63] S. A. Schumacher, J. R. Botha, V. Alberts, *Journal of Applied Physics* **2006**, *99*, 6 063508.

[64] C. F. Klingshirn, *Semiconductor Optics*, Springer Berlin Heidelberg, **2012**.

[65] A. C. Ferreira, S. Paofai, A. Létoublon, J. Ollivier, S. Raymond, B. Hehlen, B. Rufflé, S. Cordier, C. Katan, J. Even, P. Bourges, *Communications Physics* **2020**, *3*, 1.

[66] S. Poncé, M. Schlipf, F. Giustino, *ACS Energy Letters* **2019**, 456–463.

[67] H. Kim, J. Hunger, E. Cánovas, M. Karakus, Z. Mics, M. Grechko, D. Turchinovich, S. H. Parekh, M. Bonn, *Nature Communications* **2017**, *8*, 1.

[68] D. G. Thomas, J. J. Hopfield, W. M. Augustyniak, *Physical Review* **1965**, *140*, 1A A202.

[69] B. K. Meyer, H. Alves, D. M. Hofmann, W. Kriegseis, D. Forster, F. Bertram, J. Christen, A. Hoffmann, M. Straßburg, M. Dworzak, U. Haboeck, A. V. Rodina, *physica status solidi (b)* **2004**, *241*, 2 231.

[70] A. Gurskii, S. Voitikov, *Solid State Communications* **1999**, *112*, 6 339.

[71] M. Soltani, M. Certier, R. Evrard, E. Kartheuser, *Journal of Applied Physics* **1995**, *78*, 9 5626.

[72] E. Kirstein, D. R. Yakovlev, E. A. Zhukov, J. Höcker, V. Dyakonov, M. Bayer, *ACS Photonics* **2022**, *9*, 4 1375.

[73] A. M. Gilinsky, K. S. Zhuravlev, *Applied Physics Letters* **2001**, *79*, 21 3455.

[74] F. T. Rabouw, J. C. van der Bok, P. Spinicelli, B. Mahler, M. Nasilowski, S. Pedetti, B. Dubertret, D. Vanmaekelbergh, *Nano Letters* **2016**, *16*, 3 2047.

[75] D. F. Nelson, K. F. Rodgers, *Physical Review* **1965**, *140*, 5A A1667.

[76] M. A. Reshchikov, M. Z. Iqbal, H. Morkoç, S. S. Park, K. Y. Lee, *Applied Physics Letters* **2003**, *83*, 2 266.

[77] R. Dingle, *Physical Review* **1969**, *184*, 3 788.

[78] R. Sauer, W. Schmid, J. Weber, U. Rehbein, *Physical Review B* **1979**, *19*, 12 6502.

[79] C. Ran, J. Xu, W. Gao, C. Huang, S. Dou, *Chemical Society Reviews* **2018**, *47*, 12 4581.

[80] J. Yuan, D. Zhou, C. Zhuang, Y. Zhou, C. Zhang, L. Wang, M. Xiao, X. Wang, *Advanced Optical Materials* **2022**, 2200606.

[81] S. Feng, Q. Qin, X. Han, C. Zhang, X. Wang, T. Yu, M. Xiao, *Advanced Materials* **2021**, *34*, 1 2106278.

[82] Q. Tan, J.-M. Lai, X.-L. Liu, D. Guo, Y. Xue, X. Dou, B.-Q. Sun, H.-X. Deng, P.-H. Tan, I. Aharonovich, W. Gao, J. Zhang, *Nano Letters* **2022**.

[83] M. P. Mamaeva, A. Y. Samsonova, A. O. Murzin, O. A. Lozhkina, A. A. Murashkina, N. I. Selivanov, Y. V. Kapitonov, *The Journal of Physical Chemistry C* **2022**.

Table of Contents

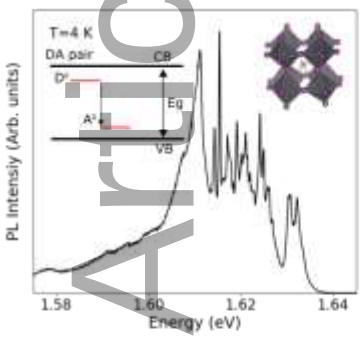

The low temperature photoluminescence of high quality $CH_3NH_3PbI_3$ perovskite single crystals is investigated. Important variations in shape and intensity of the defect emission is observed and are explained by donor-acceptor pair (DAP) recombination in presence of potential fluctuation. LO-phonon replicas of the DAP emission are evidenced. Sharp lines with sub-meV widths due to discrete DAP recombination are resolved.

LIST OF FIGURES

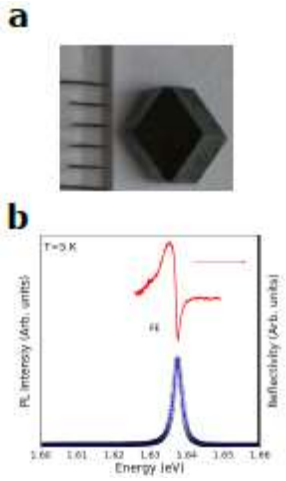

Figure 1: a) Image of a millimeter-scale crystal of $CH_3NH_3PbI_3$ b) Micro-photoluminescence and reflectivity spectra at 5K. The solid blue line is a fit with a Lorentzian function with a FWHM of 3 meV

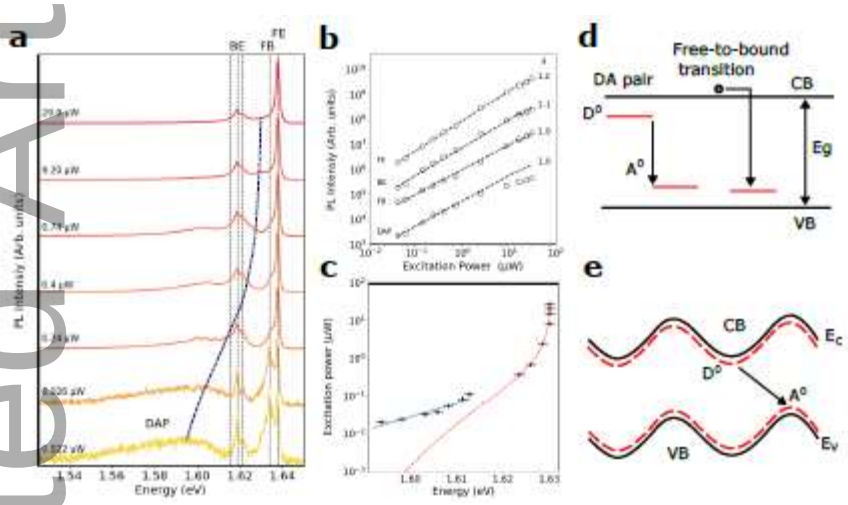

Figure 2: a) Photoluminescence spectra normalized to the maximum of the FE emission, showing the evolution of the spectral shape with excitation power. The blue dashed line serves as a guide to the eye for the evolution of the DAP band. b) PL intensity as function of excitation power for the FE (1.637 eV), BE (1.618 eV), FB (1.634 eV) and DAP emission (1.600 eV). c) Excitation power as a function of the energy of the maximum of the broadband emission. The red dashed line is a fit of the high energy range data based on equation 3. A fit of the low energy range based on equation 4 is shown with a continuous blue line. d) Schematic of donor-acceptor pair and free-to-bound in a weakly compensated semiconductor. e) DAP recombination in a strongly compensated semiconductor with potential fluctuation

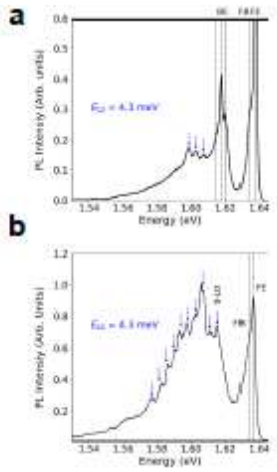

Figure 3: a) DAP emission with LO-phonon replicas acquired during the power dependent measurement, recorded at 0.24 µW b) Additional example of DAP emission with LO-phonon replicas spaced with an energy $E_{LO} = 4.3\,\text{meV}$ measured on a different crystal.

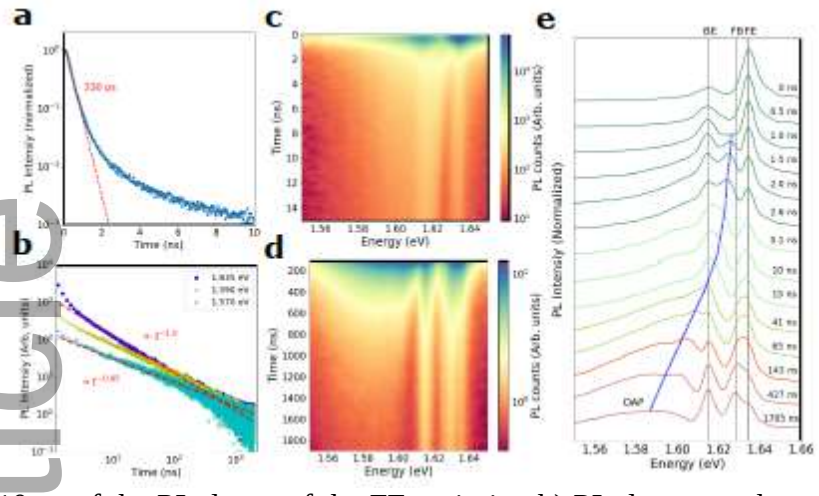

Figure 4: a) First 10 ns of the PL decay of the FE emission b) PL decays at three different energies. Red dashed lines are fit of the data with power law decay. c) Map of the PL intensity as a function of time after the excitation pulse and emission energy for the first 15 ns after the pulse. d) Map of the PL intensity as a function of time on a longer timescale. e) Normalized time-resolved spectra at different delays. The dashed blue line follows approximately the red-shift of DAP band and is a guide for the eye

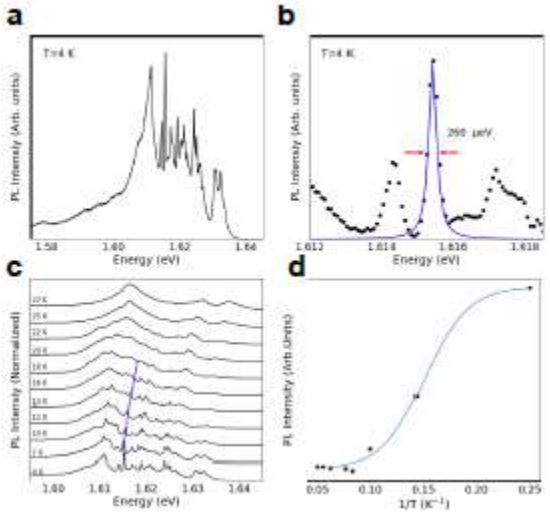

Figure 5: a) PL spectrum of a $CH_3NH_3PbI_3$ crystal showing discrete DAP lines b) PL peak centered at 1.6154 eV fitted with a Lorentzian function with a FWHM of approximately 260 µeV. c) Temperature dependence of the PL intensity d) PL integrated intensity versus temperature for the peak at 1.6154 eV. The solid line is a fit based on 6, with a thermal activation energy of $4.2 \pm 0.5\,\text{meV}$